Bio-Design and Manufacturing (2021) 4:87–99
https://doi.org/10.1007/s42242-020-00102-7

RESEARCH ARTICLE

Customized reconstructive prosthesis design based on topological optimization to treat severe proximal tibia defect

Aobo Zhang[1] · Hao Chen[1] · Yang Liu[1] · Naichao Wu[1] · Bingpeng Chen[1] · Xue Zhao[2] · Qing Han[1] · Jincheng Wang[1]

Received: 13 July 2020 / Accepted: 6 October 2020 / Published online: 13 November 2020

Abstract

A novel reconstructive prosthesis was designed with topological optimization (TO) and a lattice structure to enhance biomechanical and biological properties in the proximal tibia. The biomechanical performance was validated through finite element analysis (FEA) and biomechanical tests. The tibia with inhomogeneous material properties was reconstructed according to computed tomography images, and different components were designed to simulate the operation. Minimum compliance TO subject to a volume fraction constraint combined with a graded lattice structure was utilized to redesign the prosthesis. FEA was performed to evaluate the mechanical performances of the tibia and implants after optimization, including stress, micromotion, and strain energy. The results were analyzed by paired-samples t tests, and $p < 0.05$ was considered significant. Biomechanical testing was used to verify the tibial stresses. Compared to the original group (OG), the TO group (TOG) exhibited lower stress on the stem, and the maximum von Mises stresses were 87.2 and 53.1 MPa, respectively, a 39.1% reduction ($p < 0.05$). Conversely, the stress and strain energy on the tibia increased in the TOG. The maximum von Mises stress values were 16.4 MPa in the OG and 22.9 MPa in the TOG with a 39.6% increase ($p < 0.05$), and the maximum SED value was 0.026 MPa in the OG and 0.042 MPa in the TOG, corresponding to an increase of 61.5% ($p < 0.05$). The maximum micromotions in the distal end of the stem were 135 μm in the OG and 68 μm in the TOG, almost a 50% reduction. The stress curves of the biomechanical test coincided well with the FEA results. The TO approach can effectively reduce the whole weight of the prosthesis and improve the biomechanical environment of the tibia. It could also pave the way for next-generation applications in orthopedics surgery.

Keywords Customized reconstructive prosthesis · Topological optimization · Finite element analysis · Graded lattice · Severe bone defect · Proximal tibia

Introduction

Proximal tibia bone defects are common in patients with giant cell tumors (GCTs) [1], total knee arthroplasty (TKA) revision [2], and open injuries [3]. Traditionally, treatments include autografts, allografts, and xenografts, but they all have their limitations [4]. Bone tissue engineering is another promising approach that shows satisfactory results in repairing the bone defect [5, 6], but it still need time to apply in clinic. Nowadays, when the defect affects the normal structure and function of the knee joint, the TKA reconstruction is required. The TKA strategies can be classified into two primary types, according to the Anderson Orthopedic Research Institute (AORI) classification [7]. For patients with AORI type-2 and type-3 defects, metaphyseal sleeves or cones can be used when the proximal cortical bone and soft tissue attachments are intact [2]. For patients with AORI type-3, such as those with massive GCTs in the proximal tibia, rotating-hinge prostheses for tumors are generally considered [8].

According to Pietro et al., the failure rate of rotating-hinge knee prostheses to treat proximal tibia defects was 36.7% after a mean follow-up of 2.7 years [9]. The major causes

✉ Qing Han
my.hanqing@163.com

✉ Jincheng Wang
jinchengwang@hotmail.com

[1] Department of Orthopedics, The Second Hospital of Jilin University, Changchun 130000, China

[2] Department of Endocrinology and Metabolism, The First Hospital of Jilin University, Changchun 130000, China

of failure include soft tissue failures, aseptic loosening, and structural fracture [8]. These three causes are collectively referred to as mechanical factors that are related to inappropriate biomechanical properties of the implants, poor osseointegration, and soft tissue reconstruction between the tibia and prosthesis. Due to the restrictive design of rotating-hinge knee prostheses, an unreasonable stress concentration between the stem and bone cannot be avoided, which will lead to unsatisfactory stability and the above-mentioned complications [10]. To overcome these issues under the circumstance of intact surrounding soft tissue attachments after resection, a customized proximal tibia block combined with a standard knee joint prosthesis was designed by our team in 2015. The standard knee joint prosthesis has a better range of motion that is more similar to nature knee joint biomechanics, and the proximal tibia block can provide attachments to the collateral ligaments to maintain stability [11].

Although the new design avoids the disadvantages of the rotating-hinge knee prosthesis and brought satisfactory follow-ups of 5–8 months, there is still a mismatch in material properties between the implant and bone. The elastic modulus of the titanium alloy is 110 GPa, compared to 10–30 GPa for bone [12]. The higher elastic modulus of the implant can cause a stress shielding phenomenon that limits the transfer of load to bones [13, 14]. As a consequence, ineffective stress can cause cessation of bone growth and result in bone resorption, which may gradually weaken implant support and lead to implant loosening and bone fracture [15]. Understanding how to achieve optimized stress distribution to reduce stress shielding and promote osseointegration is needed to improve the long-term prosthesis survival rates.

Topology optimization (TO) is a method of systematically removing excess material from the design area to adjust the stress distribution and obtain higher strength-to-weight ratios [16]. With the development of additive manufacturing technology, the TO prosthesis can be manufactured to achieve personalized treatment, especially in orthopedic patients [17, 18] who have undergone resections of pelvic tumors [19], interbody cage implantation in spinal surgeries [13], and femoral stem replacement in total hip arthroplasty [20]. It is generally accepted that the application of TO can optimize prosthesis material distribution and enhance the load transfer mechanism of the implant–bone interface. Based on the TO design, the graded lattice structure can further reduce the elasticity modulus of the prosthesis and provide a microenvironment for bone ingrowth while maintaining prosthesis stability [15, 21]. To further assess design rationality, finite element analysis (FEA) is considered an effective method that can analyze physiological load simulation in complex mechanical circumstances [22].

This study proposed a novel TO prosthesis design for severe defects in the proximal tibia. In addition to maintain knee joint function and stability, the TO prosthesis could reduce weight, avoid stress shielding, and improve the biomechanical environment of the tibia. Biomechanical changes compared with the original prosthesis were analyzed by FEA and biomechanical tests.

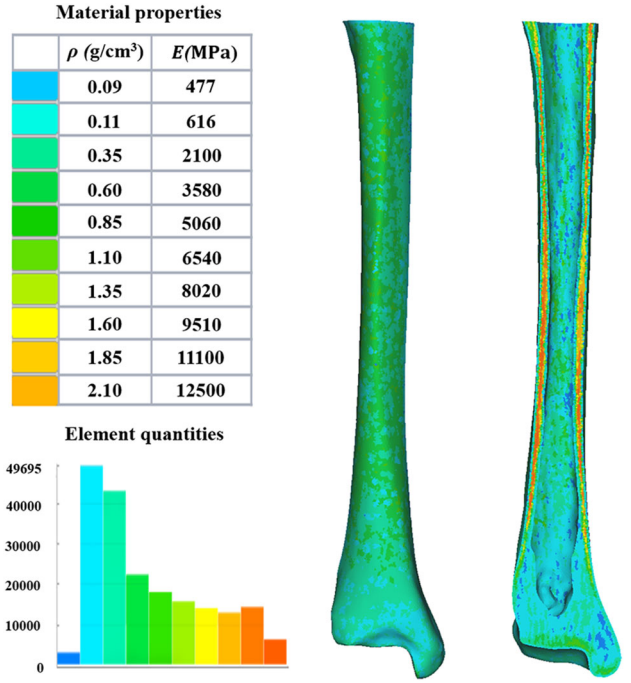

Fig. 1 Detailed material properties of the inhomogeneous femur. Ten different material properties of the tibia are distinguished by ten colors. ρ presents the bone density; E presents the elasticity modulus

Materials and methods

Inhomogeneous 3D tibia remodeling and surgical simulation

Computed tomography (CT) scan data were collected from a 40-year-old female patient with a GCT in the proximal tibia through the Philips iCT 256 CT scanner at 156 mA and 120 kVp with a slice thickness of 0.602 mm. The images were imported into *MimicsResearch* (v19.0, Materialise, Belgium) for remodeling. A threshold value of 190–210 (average 200) was selected to distinguish the bone from muscles and soft tissues. The material properties of the tibia were represented by the radiographic density of CT images, which was quantified as Hounsfield units (HU). According to the following *Mimics* formulas, the bone density (ρ) and elasticity modulus (E) of each part were calculated using a Poisson's ratio (ν) of 0.3:

$$\rho\left(\mathrm{g/m^3}\right) = -13.4 + 1017\ \mathrm{HU}, \tag{1}$$

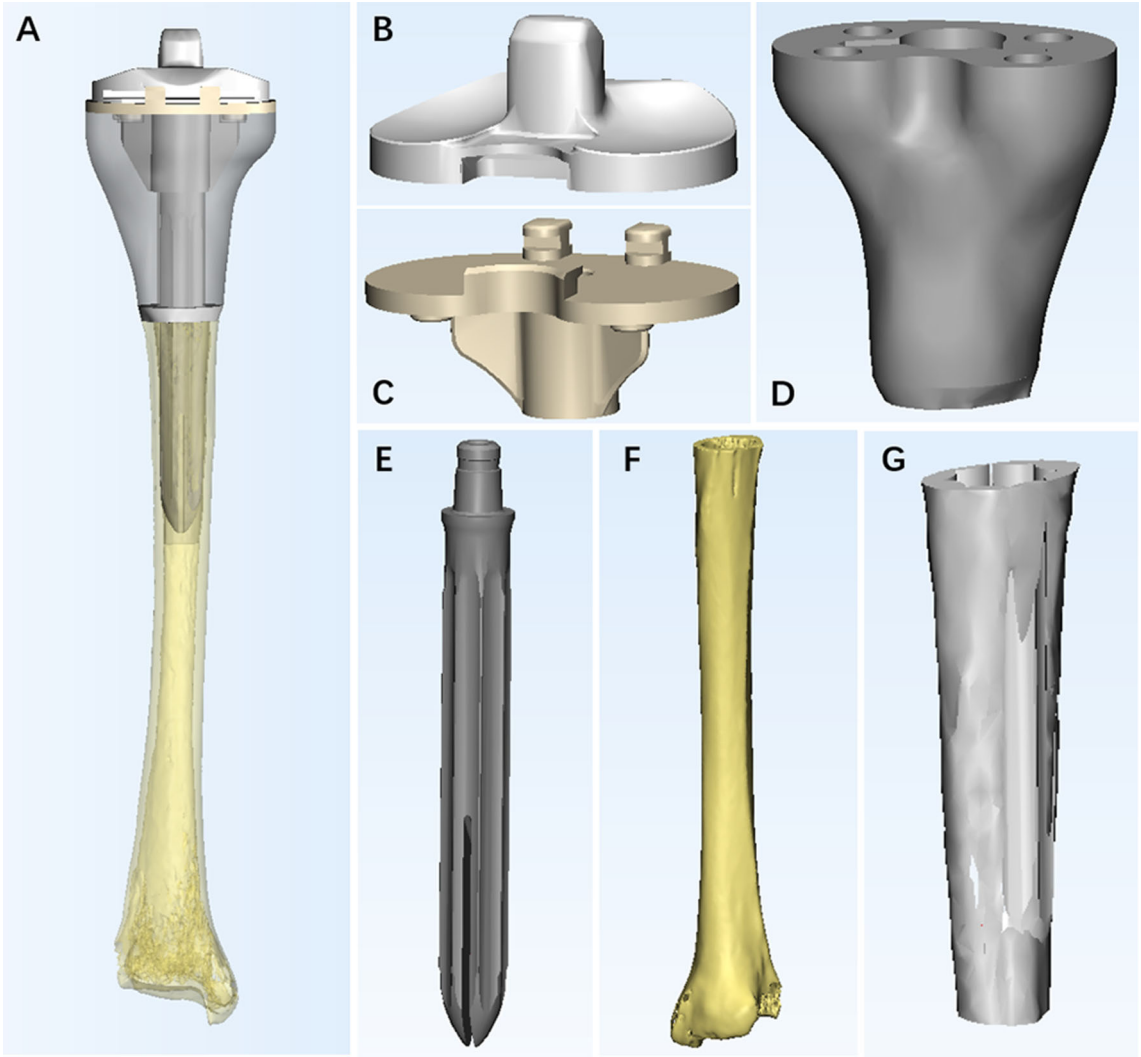

Fig. 2 The finite element models of all components. **a** All components are set and assembled to simulate the operation, **b** tibial bearing, **c** tibial tray, **d** block prosthesis, **e** stem, **f** tibia, **g** bone cement

$$E(\mathrm{Pa}) = -388.8 + 5925\rho\left(\mathrm{g/m^3}\right). \tag{2}$$

The proximal tibia with GCT was resected. The remaining tibia was divided into ten materials with different colors in order to be distinguishable: The properties and element quantities are shown in Fig. 1.

All components were prepared in *stl* format files, including the tibial bearing, tibial tray, block prosthesis, stem, bone cement, and tibia. The simulated operation was performed in *3-Matic* (v11.0, Materialise, Belgium). Every component was carefully set in the position to ensure accuracy (Fig. 2).

Gait analysis

A female patient weighing 60 kg participated completed gait analysis 6 months after surgery. A motion capture system Cortex (V5.5.0, Motion Analysis, USA) was used in this research. Six cameras covered the gait path in 360 degrees, 4 forces plates were placed under the gait path, and 19 markers were used to catch lower limbs motion (both static capture and walking capture). In static capture, the patient was required to stand on the force plates to obtain the mechanical data of leg impact. During walking capture, the patient was asked to walk at a naturally self-controlled speed along the gait path. All the data were collected and analyzed by Orthotrak (V6.6.1, Motion Analysis, USA). The longitude compression force of the knee during the entire gait cycle is shown in Fig. 3. The maximum force was 1647 N (approximated as 1650 N for subsequent analysis), which appeared at the second force peak at 40% percent of the gait cycle.

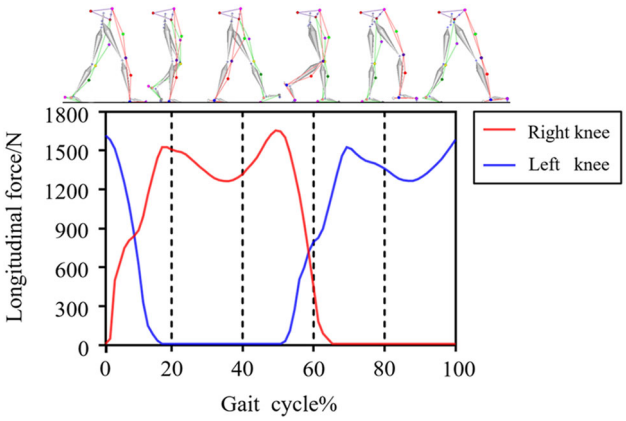

Fig. 3 The longitude compression force of the knee during the whole gait cycle. The maximum force is 1647 N, at the second force peak around 40% of the gait cycle

Finite element model establishment

HyperMesh (14.0, Altair, USA) was used to create the triangular meshes and volume meshes in an average size of 1 mm, except the stem and bone cement. Since these two components had small features, an average size of 0.4 mm was appropriate. The material properties and element quantities are shown in Table 1. Nonlinear friction with a surface-to-surface contact model was established for further analysis. The friction types between one component and another were set according to different contact surfaces as shown in Table 2. Static analysis was performed under the load condition of 1650 N on the tibia to simulate the maximum force during the entire gait cycle. The force was separated into 660 N and 990 N for the lateral and medial tibia platform since the ratio was 40%:60% according to previous studies and loaded by rigid bar element 3 (Rbe3) to evenly transfer the force [22]. The inferior surface of the distal tibia was completely constrained for all degrees of freedom (DOF) with no rotation or displacement (Fig. 4).

TO of original prosthesis

The elements connected with the tibia tray and stem were selected as the "frozen" area; the remaining elements of the prosthesis were the design area to be optimized. Minimum compliance of the TO subject to a volume fraction constraint was utilized under the loads and boundary conditions mentioned above. The optimization process was as follows:

$$\text{Objective}: \ \text{minimize}\ (U_c);$$
$$\text{Constraint}: \ 0 < \eta_i < 1\ (i = 1, 2, 3 \ldots n),$$
$$V \le V_O - V*, \tag{3}$$

Table 1 Material properties of the components

Component	Elasticity modulus (MPa)	Poisson's ratio	Element
Tibial bearing	2300	0.25	73,148
Tibial tray	114,500	0.3	79,176
Block	114,500	0.3	254,179
Stem	114,500	0.3	367,941
Cement	2150	0.3	441,424

Table 2 Friction types between components

Contact surface A	Contact surface B	Friction type
Tibial bearing	Tibial tray	Freeze
Tibial tray	Stem	Freeze
Tibial tray	Block	Stick
Block	Tibia	Stick
Stem	Cement	Stick
Tibia	Cement	Stick
Stem	Tibia	Static friction

$$V = \sum_i \eta_i V_i, \tag{4}$$
$$E_i = E(\eta_i), \tag{5}$$
$$\{\sigma_i\} = [E_i]\{\varepsilon_i\}, \tag{6}$$

where U_c is the compliance; η_i is the internal pseudo-density assigned to every finite element (i); V is the computed volume; V_O is the original volume; $V*$ is the material to be removed; V_i is the volume of element i; E_i is the elasticity modulus of every element; E is the elasticity modulus; σ_i is the stress vector of element i; ε_i is the strain vector of element i. The density η is taken as the design variable with the range of 0–1, where 0 means the material needs to be removed and 1 means the material needs to be retained. The program was set to reduce the volume up to 40% and iterate 20 times. The convergence tolerance was 0.0001.

FEA of the OG and the TOG

To verify the effect of TO and estimate stress shielding, we compared the original group (OG) and the TO group (TOG) by three indicators: stress, micromotion, and element strain energy. The results were displayed in *HyperView* (Altair, USA).

The von Mises stress was selected to discriminate regions for different stress. Five intersecting surfaces were selected every 2 cm from the contact surface of the prosthesis and tibia. The stress of the bone–implant interface can reflect the stress shielding between the bone and prosthesis. Due

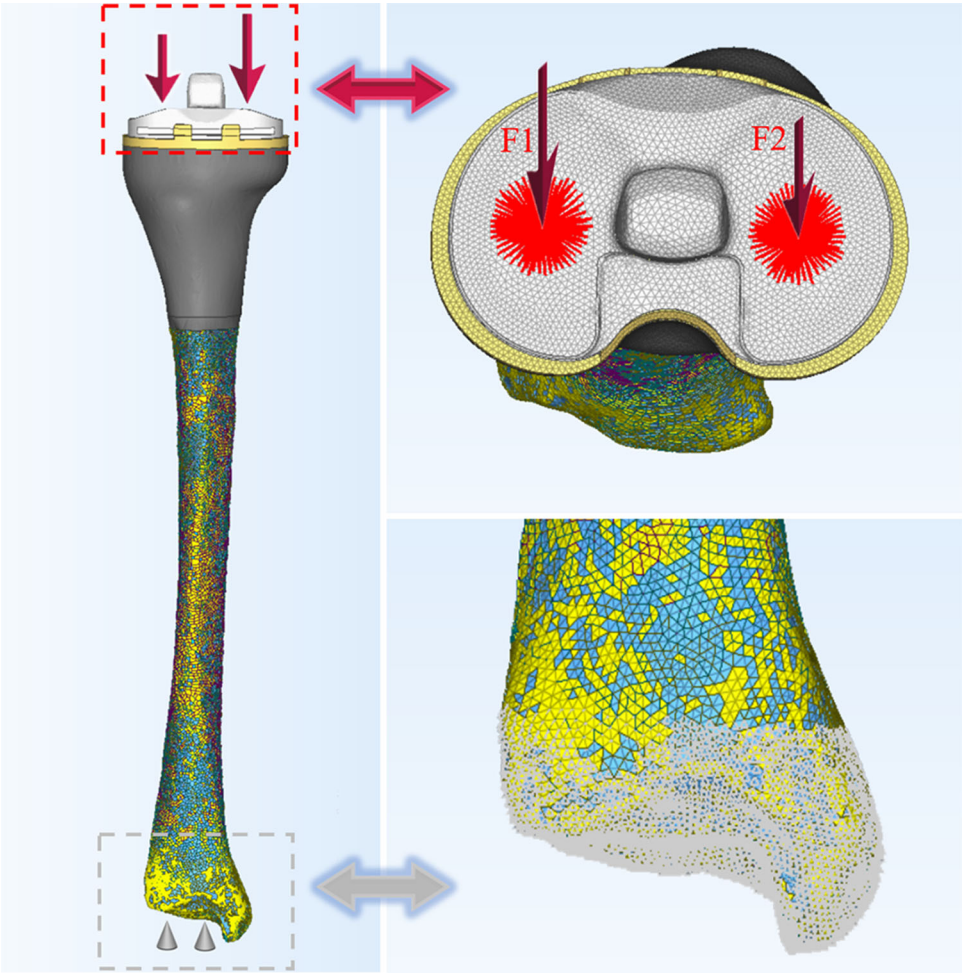

Fig. 4 The loads and constraint conditions of the tibia. The force is separated into 660 N (F2) and 990 N (F1) since the ratio of the lateral and medial tibia platform is 40%:60%. The forces are loaded through the rbe3 component to apply uniformly to each point of the stress area. The distal end of the tibia is fully constrained

to the unique shape, every intersecting surface of the stem was divided into eight parts (Fig. 5a). Every intersecting surface of the tibia was divided into four parts (Fig. 5b). The stresses of 10 elements were measured in each part, and the comparison between the OG and TOG was statistically analyzed in *SPSS* (V21.0, IBM, USA) by paired-samples *t* tests, with *p* values less than 0.05 considered significant. The stress changes on stem and tibia before and after optimization were presented using a novel graphical method.

Micromotion was defined as the relative displacement of two adjacent elements of the stem and tibia. Adjacent elements with maximum relative displacement were measured on the five intersecting surfaces mentioned above to compare the OG and TOG performances.

The strain energy density (SED) was used as mechanical stimulus and could be used as an index of stress shielding, with high SED indicating low stress shielding. Also, the SED was another proxy for bone resorption, and the results were very similar with von Mises [23–25]. In this study, the SED of the tibia was evaluated by the element strain energy and the tibial SED of the OG and TOG on the five intersecting surfaces was compared. The measurement and analysis details were the same as for stress.

TO prosthesis manufacturing

The internal lattice architecture of the prosthesis was designed by *Magics* (v21.0, Materialise, Belgium) according to the optimized results. The "Structures" function was used to establish lattice architecture without outer shell. A basic cross-type of lattice structure with the same dimensions in *X*, *Y*, and *Z* axes was designed and added to the library. The strut thickness, porosity, and pore size were constrained by the requirements of bone growth and electron beam melting (EBM). The removed part was designed in a struct thickness of 150 μm, an optimum pore size of 700 μm, and porosity of 70% to allow for soft tissues ingrowth [26]. The optimized part was designed in a struct thickness of 250 μm, a pore size of 200 μm, and porosity of 20% to assume more stress and maintain the prosthesis stability. The "frozen" part was solid that could tightly connect with the tibia tray and stem. The entire TO prosthesis was manufactured by the EBM technique (Q10 plus, Arcam AB™, Krokslatts Fabriker, Mondal,

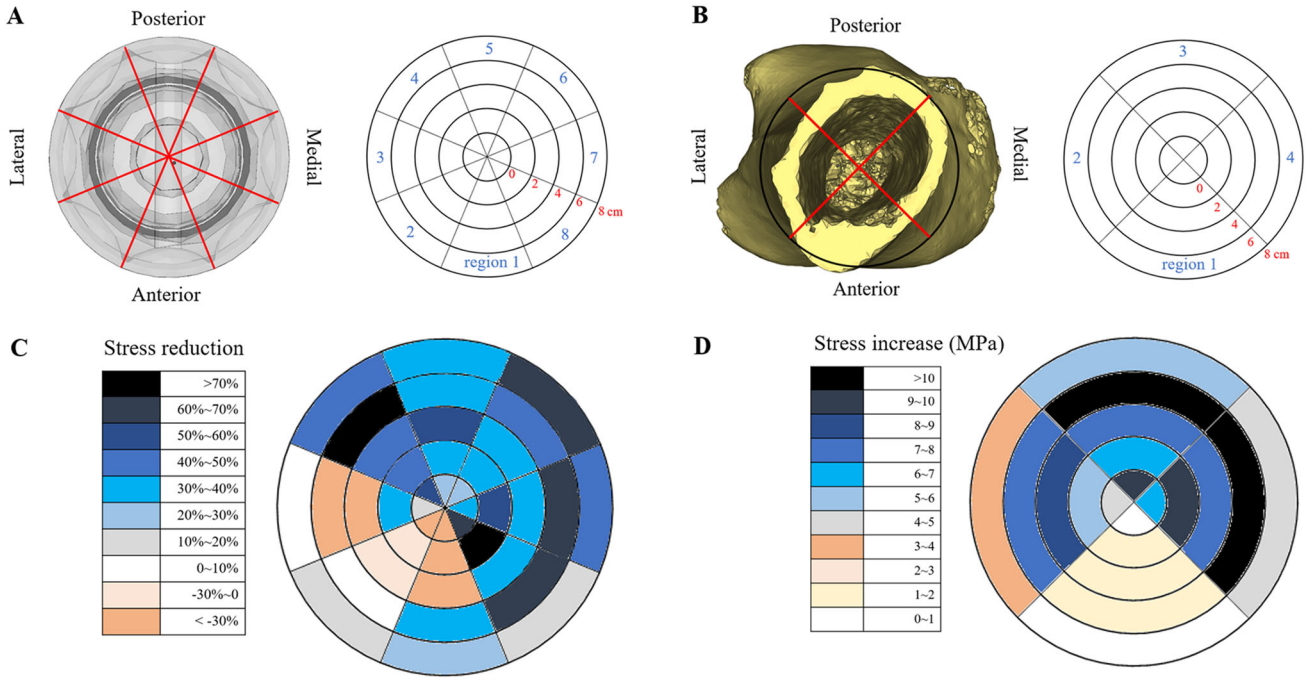

Fig. 5 The stress comparisons of the stem and tibia between OG and TOG. **a** The stem is divided into eight regions and five intersecting surfaces, **b** the tibia is divided into four regions and five intersecting surfaces, **c** the stress comparison of the stem between OG and TOG; different colors represent different degrees of stress reduction, **d** the stress comparison of the tibia between OG and TOG; different colors represent different degrees of stress increase

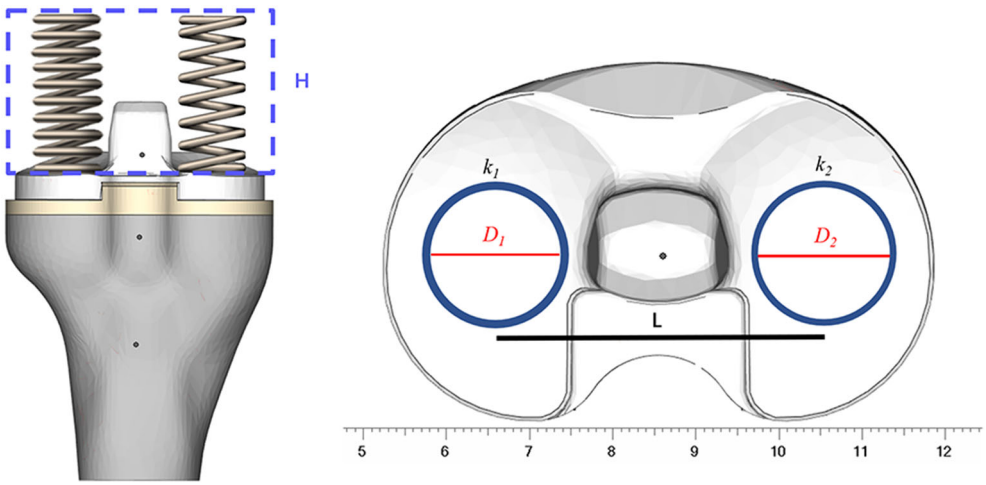

Fig. 6 Two testing springs to apply 60% and 40% of the force on the medial and lateral sides of the knee. The spring constant k is determined by: $k = G \times d^4/8 \times (N-2) \times (D-d)^3$. G: shear modulus; d: wire diameter; N: turns; D: outer diameter. $k_1 = 60$ kg/mm, $G_1 = 79{,}000$ N/mm^2, $N_1 = 10$, $D_1 = 18$ mm, $d_1 = 3.5$ mm; $k_2 = 40$ kg/mm, $G_2 = 79{,}000$ N/mm^2, $N_2 = 8$, $D_2 = 18$ mm, $d_2 = 3$ mm; H: height of the string (5 cm); L: length between two strings (4 cm)

Sweden). Inert gas was atomized, and the Arcam Ti6Al4V ELI powder particle size was 45–100 μm. The prosthesis was processed at 920 °C for 2 h.

Biomechanical test

The biomechanical tests were conducted using cadaveric tibia samples. The tibia was cut to simulate the operation and connected with the other components. The distal end of the tibia was contacted with the fixture, and quick-drying

Fig. 7 The biomechanical experiment to get the stresses of the tibia. Ten strain gages are plastered on the medial and lateral sides of the tibia every 2 cm from the contact surface between the block and tibia. 1650 N is loaded on the strings by the load-controlled system

gypsum was used for stabilization. Two testing springs with different constants ($k_1 = 60$ kg/mm, $k_2 = 40$ kg/mm) were designed to apply 60% and 40% of the force on the medial and lateral sides of the knee (Fig. 6). Ten strain gages were plastered on the medial and lateral sides of the tibia every 2 cm from the contact surface between the block and tibia. A static strain test system (v2.2.1, Test, China) was used to collect the stress data. The load-controlled system was gradually increased to 1650 N and kept there on until the data collection was finished (Fig. 7). The test was repeated three times to obtain the average stresses on the tibia. The biomechanical test results were compared with the FEA results to verify measurement accuracy.

Results

Topological optimization results and lattice design

The TO results are shown in Fig. 8. Elements with a density of > 0.25 were reserved. 62% of material in the original block in the design area was reserved to be the TO part. The newly designed TO prosthesis with the lattice structure was 77% lighter in weight.

FEA results

Stress

The comparison of the average von Mises stress distribution on the stem between the OG and TOG is shown in Fig. 9. The stresses of the stem were obviously reduced in most regions after optimization. The maximum von Mises stress values were 87.2 MPa in OG and 53.1 MPa in TOG, a 39.1% reduction. There were significant differences in all eight regions and five intersecting surfaces ($p < 0.05$); the stress changes are shown in Fig. 5c.

The comparison of the average von Mises stress distribution of the tibia in five intersecting surfaces between the OG and TOG is shown in Fig. 10. Compared with the OG, the stresses on the tibia of the TOG significantly increased in all four regions, and at all five intersecting surfaces ($p < 0.05$), the stress changes are shown in Fig. 5d. The maximum von Mises stress values were 16.4 MPa in the OG and 22.9 MPa in the TOG, a 39.6% increase.

Micromotion

The maximum relative displacement of the adjacent stem and tibia on five intersecting surfaces in both groups is presented in Table 3. The maximum micromotion of the stem was 135 μm in the OG and 68 μm in the TOG, both in the distal end. The maximum micromotion reduction was close to 50%.

SED

The comparison of SED between OG and TOG is shown in Fig. 10. The strain energy of the tibia significantly increased in all intersecting surfaces after optimization ($p < 0.05$). The maximum SED value was 0.026 MPa in the OG and 0.042 MPa in the TOG, corresponding to an increase of 61.5%.

Biomechanical test results

The stress values of the medial and lateral sides of the tibia are shown in Table 4. The maximum mean stresses of the medial

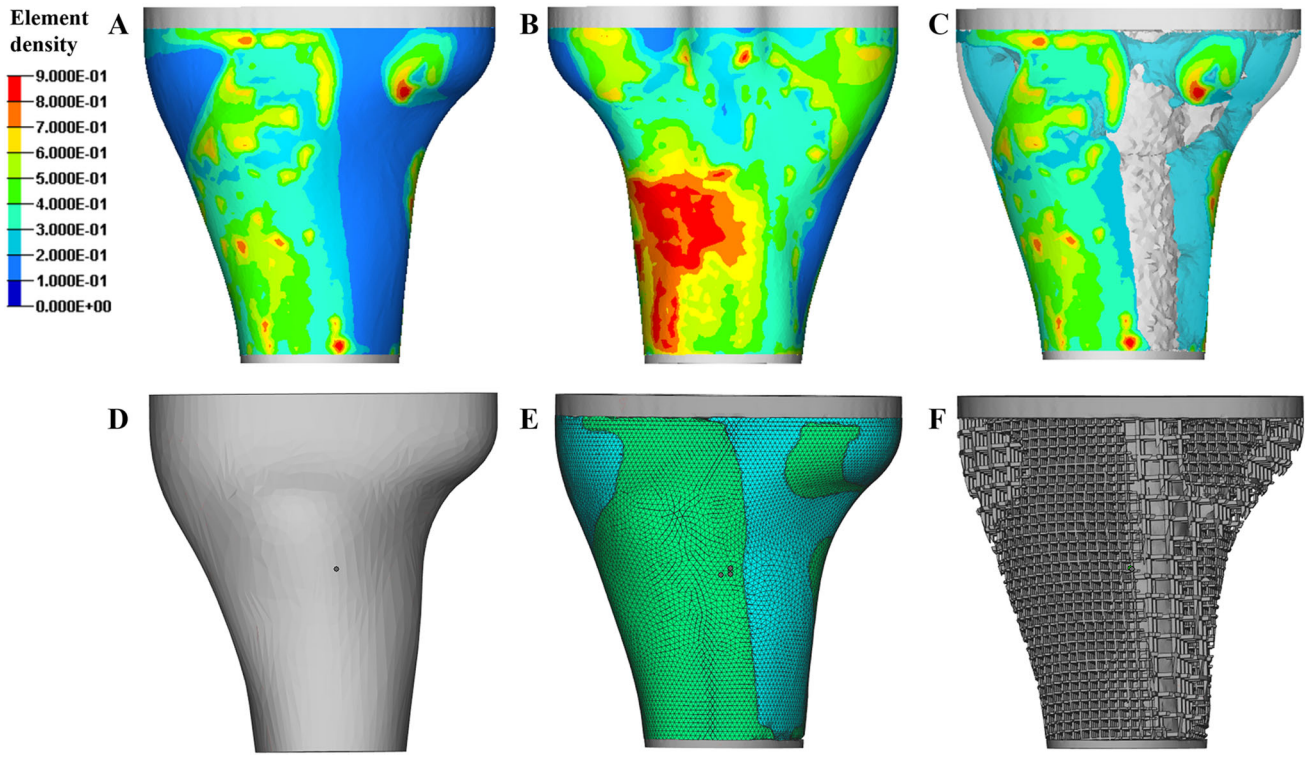

Fig. 8 Topological optimization block and the lattice structure. **a** The element density distribution of the block in the front view, **b** the element density distribution of the block in the back view, **c** the elements with a density of more than 0.25 and the "frozen" part (in color gray) are preserved to be the TO block, **d** the *stl* format of the original block, **e** the *stl* format of the frozen (in color gray), removed (in color blue), and TO part (in color green) after post-process, **f** the *stl* format of TO prosthesis with a lattice structure

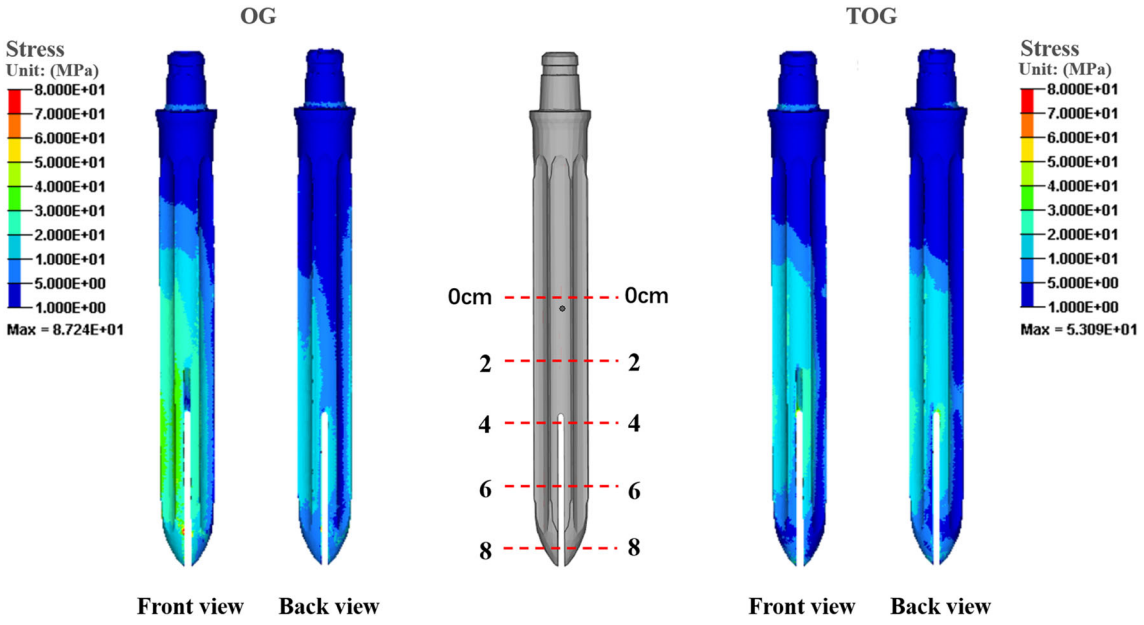

Fig. 9 Comparison of the stress distribution on the stem between OG and TOG. The maximum stress of the stem is 8.72 MPa in OG and 5.31 MPa in TOG. In most areas of the stem, the stress is decreased in TOG

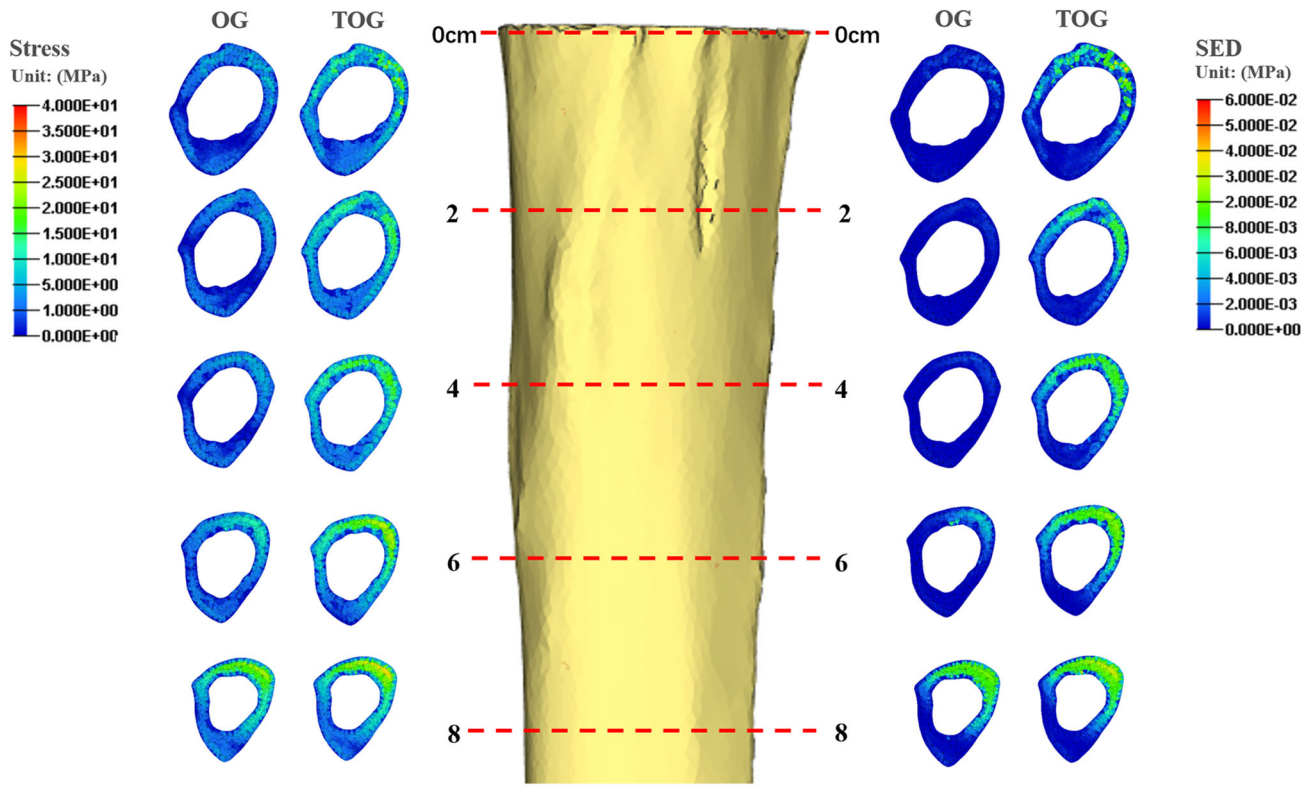

Fig. 10 Comparison of the stress and SED distribution on the tibia between OG and TOG. The stress and SED increase significantly in TOG in all five intersecting surfaces

Table 3 Maximum displacement of adjacent tibia and stem

Intersecting surfaces (cm)	Displacement in OG (mm)			Displacement in TOG (mm)		
	Tibia	Stem	Micromotion	Tibia	Stem	Micromotion
0	0.139	0.171	0.032	0.092	0.112	0.020
2	0.125	0.170	0.045	0.086	0.11	0.024
4	0.118	0.207	0.089	0.092	0.142	0.050
6	0.120	0.225	0.105	0.103	0.156	0.053
8	0.160	0.295	0.135	0.146	0.214	0.068

and lateral tibia were 3.67 ± 0.04 MPa and 2.31 ± 0.04 MPa, which appeared on the fourth intersecting surface. The comparison between the FEA results and biomechanical test results is shown in Fig. 11. The biomechanical test results increased by an average of 27% (range of 15–46%) compared with the FEA results.

Table 4 Biomechanical testing results of the stress on medial and lateral tibia

Intersecting surfaces (cm)	Medial tibia ± Std (MPa)	Lateral tibia ± Std (MPa)
0	0.47 ± 0.02	0.41 ± 0.03
2	2.64 ± 0.03	1.97 ± 0.04
4	3.02 ± 0.07	2.01 ± 0.04
6	3.67 ± 0.04	2.31 ± 0.04
8	1.05 ± 0.03	0.71 ± 0.03

Discussion

The treatment of severe proximal tibia defects remains challenging. The current strategy for patients with a proximal tibia GCT is to combine a customized titanium block with a standard knee prosthesis to be implanted after resection [11]. However, the elasticity modulus of the original prosthesis is inevitably much higher than that of bone tissue and will cause stress shielding [27]. Over time, stress shielding will lead to bone resorption and result in aseptic loosening and fracture around the prosthesis [28]. Therefore, the

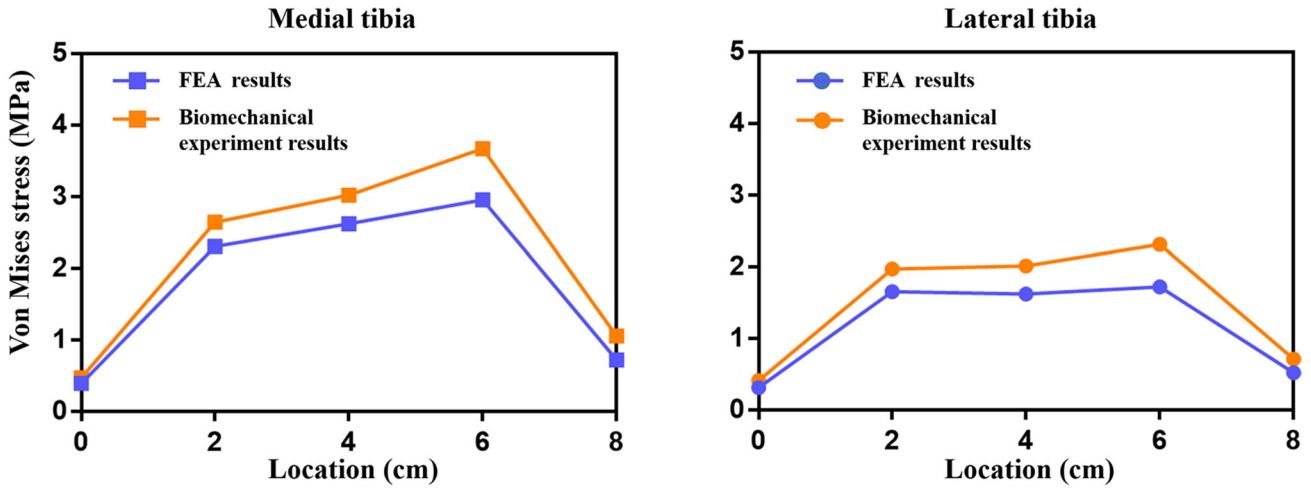

Fig. 11 Comparison between the FEA results and the biomechanical experiment results of the stress on the tibia. The stress curves of the FEA in medial and lateral tibia coincided well with the biomechanical test

emphasis of this research was to optimize the prosthesis to reduce the elasticity modulus and obtain better mechanical performance, which can increase prosthesis survival rates and enhance patient's quality of the life.

Two main strategies are generally accepted and utilized to reduce the implant's elasticity modulus. One is to change the materials, but the research and development, approval, manufacturing verification, and clinical verification processes of new materials are rigorous and time-consuming. The second is to change the implant shape or structure. Kharmanda demonstrated that the TO method could effectively reduce the elasticity modulus of the implant and avoid stress shielding [20]. Alkhatib et al. showed that a prosthesis with functionally graded material could decrease the elasticity modulus of the implant and promote bone tissue ingrowth [29]. Therefore, we adopted a TO combined with a graded lattice to change the prosthesis structure to enhance its mechanical properties and reduce stress shielding.

FEA is an effective tool to assess the mechanical properties of both the bone and prosthesis. Analysis accuracy depends on the authenticity of the finite element model. In this research, an inhomogeneous tibia model was established based on lower limb CT data. For the loading condition, previous studies mostly selected the loads data reported in the literature. However, in this study, gait analysis was performed to obtain the real forces of the tibia platform during the entire gait cycle. Shu et al. reported that the maximum medial and lateral contact forces were about 1000 N and 600 N, appeared at the second force peak in 40% gait cycle [30]. The maximum load during the entire gait cycle was 1650 N and appeared in the 40% gait cycle in this study, which was close to the results of Shu's study. The distal end of the tibia was constrained in all six DOF, including the displacement and rotation on X-, Y-, and Z-axes. Besides the loads and constraints, contact between components is also important for FEA accuracy. According to EI-Zayat et al., the presence of the cement can reduce stresses in every stem region, especially in the distal end, which can decrease stem-end pain [31]. Therefore, bone cement was used to connect different components and buffer the stress. The friction between the components and bone cement was set as "stick," between "slide" and "freeze." The friction between the stem and tibia internal interface was set in static friction with a coefficient of 0.2 [32]. The stress, displacement, and element strain energy distribution were exported as the results to evaluate TO prosthesis performance.

Besides FEA, the TO prosthesis was manufactured for biomechanical testing to further verify its performances. The static loading and constraint were consistent with the FEA simulation. Two designed springs with different constants were applied to take on different forces in the medial and lateral sides of the tibia with a force ratio of 60%:40%, the same as FEA. Due to the technical limitations, the stresses of the stem and intramedullary tibia could not be measured. Therefore, the strain gauges were plastered every 2 cm on the medial and lateral tibia surface to simulate the five intersecting surfaces.

The FEA results showed that the stress on the stem of both the OG and the TOG increased gradually from the proximal end to the distal end. The results agree with previous studies and explain why pain and fracture usually occurred on the bone connected with the distal end of the stem [31, 33]. Compared to the OG, stresses on the stem of the TOG in regions 4, 5, 6, 7, and 8 were reduced at an average range of 30–40%. Stress reduction was more obvious in the distal end, which decreased by > 60%. In regions 1, 2, and 3, the stresses increased in the first three intersecting surfaces but decreased in the distal two intersecting surfaces. Compared

with the other five regions, the stresses in these three were relatively low. After optimization, the stresses of regions 1, 2, and 3 increased by 10–40% in the first three intersecting surfaces, which made the whole stress distribution more uniform.

Conversely, stress on the tibia increased significantly in regions 2, 3, and 4, and it slightly increased in region 1. The reason might be that the position of region 1 was connected to regions 1, 2, and 3 on the stem. Since the bone cement between the regions had a buffer function, the stress increased slightly instead of decreasing. All these results indicated that more stress was transferred from the implant to the bone, and the goal of reducing stress shielding was achieved. This appropriate stress will promote bone and soft tissue growth through the lattice to connect more stably with the prosthesis [34].

The SED is another indicator for evaluating stress shielding. The difference of SED between the OG and the TOG can evaluate tibia bone resorption [24], which is the consequence of the stress shielding. In the distal two intersecting surfaces, the maximum SED value was 0.026 MPa in the OG and 0.042 MPa in the TOG, an increase of 61%. The SED distribution showed that it increased obviously in all tibia regions after optimization, which is the proof of decreased bone resorption and stress shielding.

Implant micromotion is another important evaluation associated with the prosthesis stability and postoperative pain. Previous studies indicated that interface micromotion around 40 μm could lead to partial ingrowth, while 100–150 μm was considered to prevent bone ingrowth, and exceeding 150 μm would completely inhibit bone ingrowth [23, 29]. The displacement results showed that the maximum axial micromotion of the stem was 135 μm in the OG and 68 μm in the TOG, a decrease of almost 50%. This demonstrated that the TO prosthesis could effectively prevent micromotion, promote bone ingrowth, and avoid pain for patients.

Biomechanical testing showed that the average stresses of the medial and lateral tibia from 0 to 8 cm were 2.17 MPa and 1.48 MPa, and the stress ratio was 1.47, which was in line with the force ratio. The maximum stresses of the medial and lateral tibia were 3.67 ± 0.04 MPa and 2.31 ± 0.04 MPa, respectively, on the fourth intersecting surface that was in contact with the distal end of the stem. The stresses on the same location of the tibia measured during biomechanical testing were very close to the FEA results. The stress measured by the biomechanical test increased by 27% on average. The reason might be that cadaveric sample was used in the biomechanical test rather than CT data used for FEA. Even so, the stress curves of the FEA coincided well with the biomechanical results and illustrated the similar stress distribution of the tibia, as shown in Fig. 11. The biomechanical testing results confirmed the accuracy of the FEA and verified the improved mechanical environment achieved by the TO prosthesis.

The implications of this research are promising and can serve as a multidisciplinary bridge integrating material optimization, biomechanics, additive manufacturing of 3D lattice architecture, and clinical applications. Customized design for patients with GCTs in the proximal tibia may lay the foundation for next-generation prostheses.

Conclusion

Compared with the original prosthesis, the TO prosthesis with graded lattice structure can reduce weight by 77%. Also, the stem stress and micromotion decreased, and the tibia stress and SED increased significantly, which indicated that stress shielding was effectively avoided and the biomechanical environment was improved. The novel design can reduce the risk of implant loosening and bone fracture, enhance patient's life quality, and pave the way for the next-generation applications in orthopedics surgery.

Acknowledgements This work was supported by: (1) National Natural Science Foundation of China [Grant Numbers 81802174, 81900726 & 82072456]; (2) Department of Science and Technology of Jilin Province, P.R.C [Grant Numbers 20200404202YY, 20200403086SF & 20200201453JC]; (3) Jilin Province Development and Reform Commission, P.R.C [Grant Number 2018C010]; (4) Education Department of Jilin Province, P.R.C [Grant Number JJKH20180106KJ]; (5) Administration of Traditional Chinese Medicine of Jilin Province P.R.C [Grant Number 2018115]; (6) 10th Youth Project of the First Hospital of Jilin University [Grant Number JDYY102019025]; (7) Department of Finance in Jilin Province [Grant Number 2019SCZT046]; (8) Undergraduate Teaching Reform Research Project of Jilin University [Grant Number 4Z2000610852]; (9) Key training plan for outstanding young teachers of Jilin University [Grant Number 419080520253]; (10) Bethune plan of Jilin University [Grant Number 470110000692]; (11) The major participant is Qing Han.

Author contributions AZ contributed to methodology, investigation, software, and writing—original draft; HC helped in writing—review, and editing and validation; YL contributed to software, writing—review, and editing; NW contributed to formal analysis and data curation; BC contributed to conceptualization and funding acquisition; XZ helped in funding acquisition and formal analysis; QH contributed to supervision, writing—review, and editing and funding acquisition; JW contributed to resources, project administration, and funding acquisition.

Data availability The datasets used or analyzed during the current study are available from the corresponding author on reasonable request.

Compliance with ethical standards

Conflict of interest The authors declare that there is no conflict of interest.

Ethical approval This study was approved by our internal institutional review board (No. 202 in 2018).

Informed consent The volunteer enrolled in the study provided written informed consent. Informed consent for publication was obtained from all participants.

References

1. Sung HW, Kuo DP, Shu WP, Chai YB, Liu CC, Li SM (1982) Giant-cell tumor of bone: analysis of two hundred and eight cases in Chinese patients. J Bone Joint Surg Am 64(5):755–761
2. Panegrossi G, Ceretti M, Papalia M, Casella F, Favetti F, Falez F (2014) Bone loss management in total knee revision surgery. Int Orthop 38(2):419–427. https://doi.org/10.1007/s00264-013-2262-1
3. Nizegorodcew T, Palmieri G, Peruzzi M, Galli M (2018) Allograft for the treatment of traumatic severe bone loss in the lateral femoral condyle: a case report. Injury 49(Suppl 4):S16–S20. https://doi.org/10.1016/j.injury.2018.11.037
4. Zhai M, Zhu Y, Yang M, Mao C (2020) Human mesenchymal stem cell derived exosomes enhance cell free bone regeneration by altering their miRNAs profiles. Adv Sci 7(19):2001334. https://doi.org/10.1002/advs.202001334
5. Noori A, Ashrafi SJ, Vaez-Ghaemi R, Hatamian-Zaremi A, Webster TJ (2017) A review of fibrin and fibrin composites for bone tissue engineering. Int J Nanomed 12:4937–4961. https://doi.org/10.2147/IJN.S124671
6. Wubneh A, Tsekoura EK, Ayranci C, Uludag H (2018) Current state of fabrication technologies and materials for bone tissue engineering. Acta Biomater 80:1–30. https://doi.org/10.1016/j.actbio.2018.09.031
7. Sheth NP, Bonadio MB, Demange MK (2017) Bone loss in revision total knee arthroplasty: evaluation and management. J Am Acad Orthop Surg 25(5):348–357. https://doi.org/10.5435/JAAOS-D-15-00660
8. Pala E, Trovarelli G, Calabro T, Angelini A, Abati CN, Ruggieri P (2015) Survival of modern knee tumor megaprostheses: failures, functional results, and a comparative statistical analysis. Clin Orthop Relat Res 473(3):891–899. https://doi.org/10.1007/s11999-014-3699-2
9. Pala E, Henderson ER, Calabro T, Angelini A, Abati CN, Trovarelli G, Ruggieri P (2013) Survival of current production tumor endoprostheses: complications, functional results, and a comparative statistical analysis. J Surg Oncol 108(6):403–408. https://doi.org/10.1002/jso.23414
10. Barrack RL, Lyons TR, Ingraham RQ, Johnson JC (2000) The use of a modular rotating hinge component in salvage revision total knee arthroplasty. J Arthroplasty 15(7):858–866. https://doi.org/10.1054/arth.2000.9056
11. Luo W, Huang L, Liu H, Qu W, Zhao X, Wang C, Li C, Yu T, Han Q, Wang J, Qin Y (2017) Customized knee prosthesis in treatment of giant cell tumors of the proximal tibia: application of 3-dimensional printing technology in surgical design. Med Sci Monit 23:1691–1700. https://doi.org/10.12659/msm.901436
12. Niinomi M, Liu Y, Nakai M, Liu H, Li H (2016) Biomedical titanium alloys with Young's moduli close to that of cortical bone. Regen Biomater 3(3):173–185. https://doi.org/10.1093/rb/rbw016
13. Chuah HG, Abd Rahim I, Yusof MI (2010) Topology optimisation of spinal interbody cage for reducing stress shielding effect. Comput Methods Biomech Biomed Eng 13(3):319–326. https://doi.org/10.1080/10255840903208189
14. Al-Ali MA, Al-Ali MA, Takezawa A, Kitamura M (2017) Topology optimization and fatigue analysis of temporomandibular joint prosthesis. World J Mech 7(12):323–339. https://doi.org/10.4236/wjm.2017.712025
15. Arabnejad Khanoki S, Pasini D (2012) Multiscale design and multiobjective optimization of orthopedic hip implants with functionally graded cellular material. J Biomech Eng 134(3):031004. https://doi.org/10.1115/1.4006115
16. Biyikli E, To AC (2015) Proportional topology optimization: a new non-sensitivity method for solving stress constrained and minimum compliance problems and its implementation in MATLAB. PLoS One 10(12):e0145041. https://doi.org/10.1371/journal.pone.0145041
17. Tilton M, Lewis GS, Manogharan GP (2018) Additive manufacturing of orthopedic implants. In: Li B, Webster T (eds) Orthopedic biomaterials: progress in biology, manufacturing, and industry perspectives. Springer, Cham, pp 21–55. https://doi.org/10.1007/978-3-319-89542-0_2
18. Bai L, Gong C, Chen X, Sun Y, Zhang J, Cai L, Zhu S, Xie SQ (2019) Additive manufacturing of customized metallic orthopedic implants: materials, structures, and surface modifications. Metals 9(9):1004. https://doi.org/10.3390/met9091004
19. Iqbal T, Wang L, Li D, Dong E, Fan H, Fu J, Hu C (2019) A general multi-objective topology optimization methodology developed for customized design of pelvic prostheses. Med Eng Phys 69:8–16. https://doi.org/10.1016/j.medengphy.2019.06.008
20. Kharmanda G (2016) Integration of multi-objective structural optimization into cementless hip prosthesis design: improved Austin-Moore model. Comput Methods Biomech Biomed Eng 19(14):1557–1566. https://doi.org/10.1080/10255842.2016.1170121
21. Rahimizadeh A, Nourmohammadi Z, Arabnejad S, Tanzer M, Pasini D (2018) Porous architected biomaterial for a tibial-knee implant with minimum bone resorption and bone-implant interface micromotion. J Mech Behav Biomed Mater 78:465–479. https://doi.org/10.1016/j.jmbbm.2017.11.041
22. Lin Y, Ma L, Zhu Y, Lin Z, Yao Z, Zhang Y, Mao C (2017) Assessment of fracture risk in proximal tibia with tumorous bone defects by a finite element method. Microsc Res Tech 80(9):975–984. https://doi.org/10.1002/jemt.22899
23. Fang J, Gong H, Kong L, Zhu D (2013) Simulation on the internal structure of three-dimensional proximal tibia under different mechanical environments. Biomed Eng Online. https://doi.org/10.1186/1475-925x-12-130
24. Lin CY, Hsiao CC, Chen PQ, Hollister SJ (2004) Interbody fusion cage design using integrated global layout and local microstructure topology optimization. Spine 29(16):1747–1754. https://doi.org/10.1097/01.Brs.0000134573.14150.1a
25. Fraldi M, Esposito L, Perrella G, Cutolo A, Cowin SC (2009) Topological optimization in hip prosthesis design. Biomech Model Mechanobiol 9(4):389–402. https://doi.org/10.1007/s10237-009-0183-0
26. Chimutengwende-Gordon M, Dowling R, Pendegrass C, Blunn G (2018) Determining the porous structure for optimal soft-tissue ingrowth: an in vivo histological study. PLoS One 13(10):e0206228. https://doi.org/10.1371/journal.pone.0206228
27. Belaid D, Vendeuvre T, Bouchoucha A, Bremand F, Breque C, Rigoard P, Germaneau A (2018) Utility of cement injection to stabilize split-depression tibial plateau fracture by minimally invasive methods: a finite element analysis. Clin Biomech (Bristol, Avon) 56:27–35. https://doi.org/10.1016/j.clinbiomech.2018.05.002
28. Gu S, Kuriyama S, Nakamura S, Nishitani K, Ito H, Matsuda S (2019) Underhang of the tibial component increases tibial bone resorption after total knee arthroplasty. Knee Surg Sports Traumatol Arthrosc 27(4):1270–1279. https://doi.org/10.1007/s00167-018-5309-4
29. Alkhatib SE, Tarlochan F, Mehboob H, Singh R, Kadirgama K, Harun W (2019) Finite element study of functionally graded porous femoral stems incorporating body-centered cubic structure. Artif Organs. https://doi.org/10.1111/aor.13444

30. Shu L, Yamamoto K, Yao J, Saraswat P, Liu Y, Mitsuishi M, Sugita N (2018) A subject-specific finite element musculoskeletal framework for mechanics analysis of a total knee replacement. J Biomech 77:146–154. https://doi.org/10.1016/j.jbiomech.2018.07.008
31. El-Zayat BF, Heyse TJ, Fanciullacci N, Labey L, Fuchs-Winkelmann S, Innocenti B (2016) Fixation techniques and stem dimensions in hinged total knee arthroplasty: a finite element study. Arch Orthop Trauma Surg 136(12):1741–1752. https://doi.org/10.1007/s00402-016-2571-0
32. Totoribe K, Chosa E, Yamako G, Hamada H, Ouchi K, Yamashita S, Deng G (2018) Finite element analysis of the tibial bone graft in cementless total knee arthroplasty. J Orthop Surg Res 13(1):113. https://doi.org/10.1186/s13018-018-0830-1
33. Jones RE, Skedros JG, Chan AJ, Beauchamp DH, Harkins PC (2001) Total knee arthroplasty using the S-ROM mobile-bearing hinge prosthesis. J Arthroplasty 16(3):279–287. https://doi.org/10.1054/arth.2001.21498
34. Wiskott HWA, Belser UC (1999) Lack of integration of smooth titanium surfaces: a working hypothesis based on strains generated in the surrounding bone. Clin Oral Implants Res 10(6):429–444. https://doi.org/10.1034/j.1600-0501.1999.100601.x